Fresnel Microfacet BRDF:
Unification of Polari-Radiometric Surface-Body Reflection

Tomoki Ichikawa   Yoshiki Fukao   Shohei Nobuhara   Ko Nishino
Graduate School of Informatics, Kyoto University
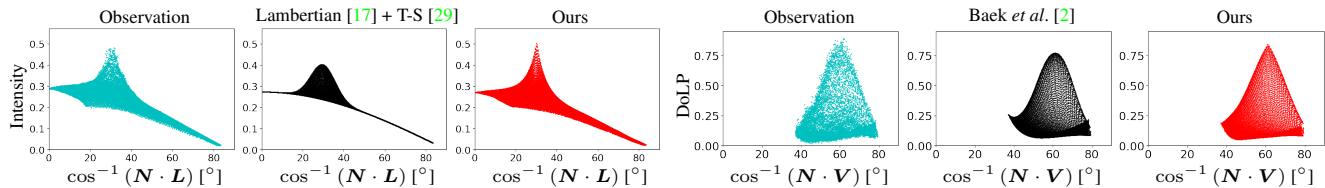https://vision.ist.i.kyoto-u.ac.jp/

Figure 1. We derive Fresnel Microfacet BRDF, a novel physically-based BRDF model which consolidates radiometric (left) and polarimetric (right) reflection as well as body and surface reflections of surface microgeometry in a single model. The model outperforms past physically-based models (*e.g.*, Lambertian [17] plus Torrance-Sparrow [29] and pBRDF [2]) in accuracy and generality.

Abstract

Computer vision applications have heavily relied on the linear combination of Lambertian diffuse and microfacet specular reflection models for representing reflected radiance, which turns out to be physically incompatible and limited in applicability. In this paper, we derive a novel analytical reflectance model, which we refer to as Fresnel Microfacet BRDF model, that is physically accurate and generalizes to various real-world surfaces. Our key idea is to model the Fresnel reflection and transmission of the surface microgeometry with a collection of oriented mirror facets, both for body and surface reflections. We carefully derive the Fresnel reflection and transmission for each microfacet as well as the light transport between them in the subsurface. This physically-grounded modeling also allows us to express the polarimetric behavior of reflected light in addition to its radiometric behavior. That is, FMBRDF unifies not only body and surface reflections but also light reflection in radiometry and polarization and represents them in a single model. Experimental results demonstrate its effectiveness in accuracy, expressive power, image-based estimation, and geometry recovery.

1. Introduction

Reflection is a fundamental physical phenomenon of light that serves as a key creator of our rich visual world. Models of light reflection lie at the heart of visual information processing both for synthesis and analysis. In computer vision, reflectance models play an essential role in 3D reconstruction, inverse rendering, and material estimation. The goal is to invert light reflection to deduce its physical ingredients, such as the surface geometry, from images. Naturally, devising simple yet accurate models that are faithful to the underlying physics becomes vital. Analytical models provide a sound basis for solving these inverse problems as parameter estimation and physically-based models lend semantic interpretations of the results.

Physically-based analytical reflectance models have been studied extensively. Parametric representations of the Bidirectional Reflectance Distribution Function (BRDF) are of particular importance, as they enable pixel-wise estimation of its parameters. Most models widely adopted in computer vision are built on two representative models corresponding to the two distinct reflection components, namely body reflection and surface reflection. Body reflection refers to the light that transmits into the subsurface and is eventually emitted from the surface. It is also called diffuse reflection as it is comparatively scattered in directions. The Lambertian reflectance model [17] which models it as uniform distribution in the angular domain dominates computer vision applications due to its simple linear form.

Surface reflection is the light that immediately reflects off the surface. It is also referred to as specular reflection as it primarily concentrates around the perfect mirror reflection direction of incident light. Torrance and Sparrow [29] introduced the idea of modeling the microgeometry within a single pixel that causes this angular spread of surface reflec-

tion with oriented mirror microfacets. Then on, many models have built on this key idea of oriented microfacets [5,30]. Oren and Nayar [22] applied the idea to body reflection by assuming Lambertian instead of mirror microfacets.

A linear combination of these diffuse and specular reflection models, most often Lambertian or Oren-Nayar plus Torrance-Sparrow, have been widely used in vision applications. There are, however, three problems that fundamentally limit the accuracy of such a reflection representation. The first is that the two reflection components are modeled on inconsistent microgeometry. Lambertian and other body reflection models assume a single Lambertian microfacet or an oriented distribution of Lambertian microfacets [22], while specular reflection models assume mirror microfacets [29]. This is physically implausible and also hinders physical interpretation of the parameter estimates.

The second is that past diffuse reflection models do not account for light transport inside the microgeometry. The Oren-Nayar model ignores discrepancies in incident and exitant microfacets. This can be fine for mesoscopic and macroscopic geometry (*i.e.*, Bidirectional Texture Function) as demonstrated in their work [22], but leads to significant inaccuracy for microgeometry (*i.e.*, regular imaging conditions). Incident light to one microfacet will likely exit from a different microfacet whose effect cannot be ignored for accurate body reflection representation.

The third is that estimation of the parameter values (*i.e.*, reflectometry) of such linear combinations of diffuse and specular reflection models is inherently unstable. Specular reflection is usually either sparse (*e.g.*, a shiny surface with a narrow highlight) or weak (*e.g.*, a rough surface with a broad specular lobe). This makes estimation of specular parameter values while disentangling diffuse and specular components challenging. Most works thus require multiple images captured from different imaging conditions.

In this paper, we derive a novel analytical reflectance model that is physically accurate and generalizes to various real-world surfaces. Our key idea is to build up from the very atomic behavior of light reflection, namely Fresnel reflection. We model surface microgeometry with a collection of oriented mirror facets, both for body and surface reflections. We carefully derive the Fresnel reflection and transmission for each microfacet as well as the light transport between them in the subsurface. By modeling the full Fresnel behavior of light for an analytically oriented distribution of mirror microfacets, we arrive at a generalized reflection model that subsumes past representative models as special cases. This physically-grounded modeling allows us to describe the polarimetric behavior of reflected light by a rough surface, in addition to its radiometric behavior. As a result, our novel reflectance model, which we refer to as Fresnel Microfacet BRDF model (FMBRDF), unifies not only body and surface reflections but also light reflection in

Model	MSR	MBR	FT	MLT	Pol.
T-S [29] + Lambertian	✓				
T-S [29] + O-N [22]	✓	✓			
Baek *et al.* [2]	✓		✓		✓
Ours	✓	✓	✓	✓	✓

Table 1. Our Fresnel Microfacet BRDF model is, to our knowledge, the first physically-based reflection model that accurately expresses microfacet surface reflection (MSR), microfacet body reflection (MBR), Fresnel transmission (FT), microscopic light transport (MLT), and polarization (Pol.) in a single model.

radiometry and polarization in a single model.

We experimentally validate our FMBRDF model by evaluating its accuracy with a wide range of measured BRDFs and images of real surfaces. The results show that FMBRDF can accurately model both the intensity and polarization, particularly in comparison with past representative models. We also show that FMBRDF can be estimated from a single polarimetric image. In the supplemental material, we demonstrate the use of FMBRDF for joint estimation of reflectance and geometry from multiple images taken under different light source directions.

To the best of our knowledge, FMBRDF is the first reflectance model to seamlessly unify body and surface reflections with the same microgeometry and also describe both its radiometric and polarimetric light reflections in a single model. We believe FMBRDF will provide an invaluable basis for accurate radiometric and polarimetric image analysis and serve as a backbone for a wide range of computer vision applications. All code and data can be found on our project page.

2. Related Works

Light reflection at a surface point can be described by the Bidirectional Reflectance Distribution Function (BRDF): the ratio of the reflected surface radiance to the incident irradiance [20]. Various models have been introduced to approximate the BRDF of real-world surfaces. Table 1 summarizes the fundamental differences between our model and representative physically-based models.

Phenomenological Models: Various empirical models have been introduced in the past. Phong [23] proposed a specular reflection model based on the power of the angle made by the mirror reflected incident light direction and the viewing direction. Lafortune *et al.* [16] generalized the Phong model with multiple specular lobes. Koenderink and van Doorn [14] used Zernike polynomials, Ramamoorthi and Hanrahan [24] spherical harmonics, and Edwards *et al.* [7] 2D Gaussians on halfway disks to describe a BRDF with basis expansion. These models are phenomenological and do not describe the physical light interaction.

Data-driven Models: Inductive reflectance models can also be derived by fitting to measurement data. Matusik

et al. [19] introduced a data-driven non-parametric reflection model using nonlinear dimensionality reduction of 100 measured BRDFs. Nishino [21] introduced the directional statistical BRDF model by viewing reflected light as a hemispherical statistical distribution. Romeiro *et al.* [25] applied non-negative matrix factorization to the angular tabulation of BRDFs. More recently, Chen *et al.* [4] derived the iBRDF model based on an invertible neural network. These data-driven models are expressive, especially when modeling those BRDFs in the vicinity of the training data, but do not offer physical interpretations of the surface. Their generalizability also solely hinges on the ability to collect dense angular measurements of the actual BRDF.

Physically-based Models: Deriving an analytical expression of the physical process of light reflection at a surface point has been a long-standing problem. Torrance and Sparrow [29] introduced the idea of modeling the microgeometry of a surface with a distribution of oriented microfacets each of which mirror-reflects light. Cook and Torrance [5] extended it with the Beckmann distribution to model wavelength-dependency. Walter *et al.* [30] applied the Cook-Torrance model to model refractive transmission of translucent materials. Holzschuch and Pacanowski [9] modeled specular reflection by combining reflection on microgeometry and diffraction on nanogeometry. Oren and Nayar [22] generalized the Lambertian model by modeling the surface microgeometry with microfacets of purely Lambertian reflection. These models, however, do not model the full BRDF and should not be simply combined (see Sec. 1).

Polarimetric Reflection Model: Polarimetric reflection models have been introduced mainly for geometry recovery from polarization. Atkinson and Hancock [1] assume pure diffuse reflection to estimate the zenith angles of surface normals from observed degrees of polarization. Others assume either pure diffuse or mirror reflection [11, 18, 28, 31]. Baek *et al.* [2] introduced a polarimetric BRDF (pBRDF) model consisting of both diffuse and specular reflections, the latter of which is based on microfacet geometry (*i.e.*, a polarimetric version of Lambertian plus Torrance-Sparrow). Extensions of this model with a unpolarized diffuse term [15] and a single scattering term [10] have been introduced. These models, however, consider diffuse reflection on a perfectly flat surface, and require special imaging setups (*e.g.*, co-axial imaging [2]) for parameter estimation. Baek *et al.* [3] acquired a pBRDF dataset consisting of 25 materials and introduced a data-driven pBRDF model.

3. Radiometric Fresnel Microfacet BRDF

We first derive the radiometric FMBRDF, the intensity behavior of our novel reflectance model, by expressing the surface and body reflections caused by the same microgeometry consisting of mirror microfacets.
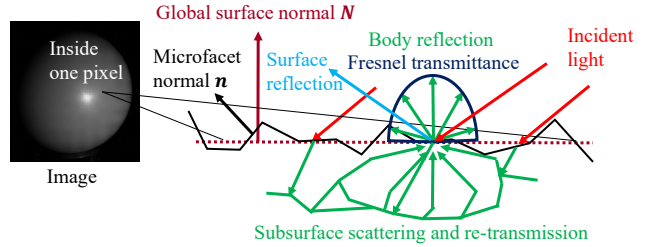

Figure 2. We model the surface microgeometry with a collection of statistically oriented mirror microfacets. Our model accurately captures both the Fresnel reflection (*i.e.*, mirror reflection) and Fresnel transmission and re-transmission (*i.e.*, body reflection) by each microfacet. Light transmitted into the surface body can be re-transmitted from a microfacet different from the incident one after scattering in the body. We also model this light transport inside the microgeometry.

As depicted in Fig. 2, a single pixel spans an area on the surface. We model the microgeometry in this surface area with a collection of oriented planar microfacets, each of which is perfectly smooth and mirror-reflects light. If we refer to the overall surface normal of this surface area as the global surface normal N, this means that N actually consists of many microfacets each with its own surface normal n oriented according to a statistical distribution. We model the Fresnel reflection and transmittance by each of these mirrored microfacets and express the aggregated reflections by the set of microfacets as surface reflection and body reflection. In contrast, past physically-based models assumed mirrored microfacets for specular reflection and Lambertian microfacets for diffuse reflection, *i.e.*, they had mismatched assumptions on the atomic behavior of individual microfacets.

3.1. Generalized Radiometric Surface Reflection

Surface reflection is the aggregated light bundle each of whose constituent light ray is mirror-reflected by the interface of a microfacet. We follow, but significantly extend, the Torrance-Sparrow model [29] to derive an expression that accurately represents this surface reflection based on the fundamental behavior of light reflection, namely Fresnel reflection.

The incident light as a bundle of uni-directional light rays cut by the surface area corresponding to a single pixel is mirror-reflected by microfacets whose normals happen to be aligned with the bisector of the view direction V and the incident light direction L, which is represented by the halfway vector $H = (L + V)/\|L + V\|$. The aggregated radiance L_s of such reflected light by a distribution of oriented microfacets becomes

$$L_s = k_s \frac{R(\theta_d)D(\theta_H)G(H)}{4(N \cdot V)} E_o \,, \qquad (1)$$

where $\boldsymbol{N}$ is the global surface normal at a pixel, k_s is the surface reflection albedo, θ_d is incident light angle to the microfacet, $R(\theta_d)$ is the Fresnel reflectance, $\theta_{\boldsymbol{H}}$ is the zenith angle of $\boldsymbol{H}$ from $\boldsymbol{N}$, D is the microfacet distribution, G is the geometric attenuation factor, and E_o is the irradiance from the light source when the surface normal is aligned with $\boldsymbol{L}$ [29]. For simplicity, we omit $\boldsymbol{N}$, $\boldsymbol{L}$, and $\boldsymbol{V}$ from the notations. While G is derived from V-cavity microgeometry in Torrance-Sparrow model [29], we instead use Smith's masking function and the separable masking-shadowing function [8, 27].

In the Torrance-Sparrow model, D is a Gaussian and its parameter σ represents the surface roughness. Nishino introduced the use of an exponential power distribution as the basis of his directional statistics BRDF model [21], which has also been adopted for modeling the microfacet orientation distribution [9]. Similarly, we model the orientation distribution D with the generalized normal distribution

$$D(\theta_{\boldsymbol{H}}) \propto \exp\left[-(\theta_{\boldsymbol{H}}/\alpha)^\beta\right] . \qquad (2)$$

Image-based measurement of such a generic microfacet orientation distribution would be impossible with a radiometric BRDF model due to the entanglement of surface and body reflections. We later show that modeling the polarimetric light behavior enables its robust estimation.

3.2. Generalized Radiometric Body Reflection

Let us first review foundational models of diffuse reflection, to derive an accurate model of body reflection by mirror microfacets, *i.e.*, the light that first transmits into the microfacet with Fresnel transmittance before reemerging. Lambert expressed the phenomenological body reflection as angularly uniform "diffuse" reflection. Oren and Nayar [22] extended this by devising a Gaussian microfacet orientation distribution similar to the Torrance-Sparrow model, but by assuming each microfacet to realize pure Lambertian reflection. In this model, the radiance observed from a surface patch is the average of the projected radiance of the microfacets weighted by the slope-area distribution. The projected radiance L_{rp} of each microfacet is defined as

$$L_{rp}(\boldsymbol{n}) = \frac{d\Phi_r(\boldsymbol{n})}{(\boldsymbol{n} \cdot \boldsymbol{N})dn(\boldsymbol{N} \cdot \boldsymbol{V})d\omega_r} , \qquad (3)$$

where $\boldsymbol{n}$ is the normal of the microfacet, $d\Phi_r(\boldsymbol{n})$ is the flux in the viewer direction, dn is the microfacet area, and $d\omega_r$ is an infinitesimal solid angle to the viewer direction. The reflected flux $d\Phi_r(\boldsymbol{n})$ is given by Lambertian reflection.

The projected radiance is weighted by the slope-area distribution, *i.e.*, the foreshortened microfacet areas

$$L_b = \int_\Omega L_{rp}(\boldsymbol{n})D(\theta_{\boldsymbol{n}})\cos\theta_{\boldsymbol{n}}d\omega_{\boldsymbol{n}} , \qquad (4)$$

where $\theta_{\boldsymbol{n}}$ is the zenith angle of $\boldsymbol{n}$ from the global surface normal $\boldsymbol{N}$, Ω is the upper hemisphere around $\boldsymbol{N}$, $d\omega_{\boldsymbol{n}}$ is an infinitesimal solid angle subtended by the microfacet normal direction. The slope-area distribution is normalized by

$$\int_\Omega D(\theta_{\boldsymbol{n}})\cos\theta_{\boldsymbol{n}}d\omega_{\boldsymbol{n}} = 1 . \qquad (5)$$

In the Oren-Nayar model, the slope-area distribution is a Gaussian function.

The Oren-Nayar model, however, has a few shortcomings as a body reflection model as we reviewed in Sec. 1. Its key assumption of Lambertian microfacets is fundamentally incompatible with specular reflection models which rightly assume mirror microfacets. In fact, it is not clear how a Lambertian microfacet can be realized in the real world, as Lambertian reflection can only result from rough surfaces (*i.e.*, it cannot be an atomic behavior of light). The original work [22] fits the Oren-Nayar model to mean intensity values of a large surface patch similar to celestial imaging conditions (*e.g.*, lunar photography), effectively demonstrating its use as a Bidirectional Texture Function (BTF) [6] not a BRDF. In other words, it models the reflectance of meso/macrogeometry by assuming Lambertian microgeometry, not individual microfacets. This renders its use for BRDF modeling and per-pixel inverse rendering inappropriate for ordinary imaging conditions. Furthermore, it does not model the light transport between microfacets. This is actually essential to realize Lambertian reflection.

Let us now derive our body reflection model based on the exact same microgeometry underlying the surface reflection. Unlike the Oren-Nayar derivation, we must consider all combinations of incident and outgoing points within the microgeometry of a pixel A_p to accommodate light transport between microfacets. We first focus on a point $\boldsymbol{p}$ on an oriented microfacet of normal $\boldsymbol{n}$ in A_p. We can rewrite $L_{rp}(\boldsymbol{n})$ with the projected radiance $L_{rp}(\boldsymbol{p}; \boldsymbol{n})$ at $\boldsymbol{p}$ as

$$L_{rp}(\boldsymbol{n}) = \frac{1}{|A_{\boldsymbol{n}}|}\int_{A_{\boldsymbol{n}}} G_m^b(\boldsymbol{p}; \boldsymbol{n})L_{rp}(\boldsymbol{p}; \boldsymbol{n})dA_{\boldsymbol{n}} , \qquad (6)$$

where $G_m^b(\boldsymbol{p}; \boldsymbol{n})$ is a binary masking function at $\boldsymbol{p}$, $A_{\boldsymbol{n}}$ is the region of microfacets oriented to $\boldsymbol{n}$ in A_p, $|\cdot|$ denotes the area of a region, and $dA_{\boldsymbol{n}}$ is an infinitesimal area in the vicinity of $\boldsymbol{p}$. The microfacets area $|A_{\boldsymbol{n}}|$ becomes

$$|A_{\boldsymbol{n}}| = |A_p|D(\theta_{\boldsymbol{n}})d\omega_{\boldsymbol{n}} . \qquad (7)$$

Similar to Eq. (3), $L_{rp}(\boldsymbol{p}; \boldsymbol{n})$ is defined by

$$L_{rp}(\boldsymbol{p}; \boldsymbol{n}) = \frac{d\Phi_r(\boldsymbol{p}; \boldsymbol{n})}{(\boldsymbol{n} \cdot \boldsymbol{N})dA_{\boldsymbol{n}}(\boldsymbol{N} \cdot \boldsymbol{V})d\omega_r} , \qquad (8)$$

where $d\Phi_r(\boldsymbol{p}; \boldsymbol{n})$ is the flux in the viewer direction at point $\boldsymbol{p}$ and $d\omega_r$ is an infinitesimal solid angle to the viewer direction. The flux $d\Phi_r(\boldsymbol{p}; \boldsymbol{n})$ is represented with the radiance

$L_r(\boldsymbol{p}; \boldsymbol{n})$ to the viewer direction at $\boldsymbol{p}$ as

$$d\Phi_r(\boldsymbol{p}; \boldsymbol{n}) = L_r(\boldsymbol{p}; \boldsymbol{n}) \cdot (\boldsymbol{n} \cdot \boldsymbol{V}) dA_{\boldsymbol{n}} d\omega_r . \qquad (9)$$

The outgoing light $L_r(\boldsymbol{p}; \boldsymbol{n})$ at a point $\boldsymbol{p}$ is the sum of the light transported from other incident points on the microgeometry. We define $dL_r(\boldsymbol{p}, \boldsymbol{p}_i; \boldsymbol{n}, \boldsymbol{n}_i)$ as the radiance of light transported from an incident point $\boldsymbol{p}_i$ on a microfacet oriented to $\boldsymbol{n}_i$. Assuming that the surface is opaque enough so that no light is transported from outside of the patch A_p, we can express $dL_r(\boldsymbol{p}; \boldsymbol{n})$ with $dL_r(\boldsymbol{p}, \boldsymbol{p}_i; \boldsymbol{n}, \boldsymbol{n}_i)$ as

$$dL_r(\boldsymbol{p}; \boldsymbol{n}) = \int_\Omega \int_{A_{\boldsymbol{n}_i}} \frac{dL_r(\boldsymbol{p}, \boldsymbol{p}_i; \boldsymbol{n}, \boldsymbol{n}_i)}{d\omega_{\boldsymbol{n}_i} dA_{\boldsymbol{n}_i}} dA_{\boldsymbol{n}_i} d\omega_{\boldsymbol{n}_i} , \qquad (10)$$

where $d\omega_{\boldsymbol{n}_i}$ is an infinitesimal solid angle that represents the normal direction $\boldsymbol{n}_i$ of an incident microfacet, $dA_{\boldsymbol{n}_i}$ is an infinitesimal area in the vicinity of $\boldsymbol{p}_i$, $A_{\boldsymbol{n}_i}$ is the region of microfacets oriented to $\boldsymbol{n}_i$ in A_p, and its area $|A_{\boldsymbol{n}_i}|$ is obtained by

$$|A_{\boldsymbol{n}_i}| = |A_p| D(\theta_{\boldsymbol{n}_i}) d\omega_{\boldsymbol{n}_i} . \qquad (11)$$

The incident flux $\Phi_i(\boldsymbol{p}_i; \boldsymbol{n}_i)$ at $\boldsymbol{p}_i$ is scattered and distributed to other points on other microfacets near $\boldsymbol{p}_i$. To represent outgoing radiance $dL_r(\boldsymbol{p}, \boldsymbol{p}_i; \boldsymbol{n}, \boldsymbol{n}_i)$ with the incident flux $d\Phi_i(\boldsymbol{p}_i; \boldsymbol{n}_i)$ at $\boldsymbol{p}_i$, we define $S(\boldsymbol{p}, \boldsymbol{p}_i; \boldsymbol{n}, \boldsymbol{n}_i)$ as

$$S(\boldsymbol{p}, \boldsymbol{p}_i; \boldsymbol{n}, \boldsymbol{n}_i) = \frac{dL_r(\boldsymbol{p}, \boldsymbol{p}_i; \boldsymbol{n}, \boldsymbol{n}_i)}{d\Phi_i(\boldsymbol{p}_i; \boldsymbol{n}_i)} . \qquad (12)$$

It describes how much light is transmitted into the surface, transported from $\boldsymbol{p}_i$ to $\boldsymbol{p}$, and re-transmitted into the air. We can decompose it into transmission, light transport, and re-transmission terms and obtain

$$S(\boldsymbol{p}, \boldsymbol{p}_i; \boldsymbol{n}, \boldsymbol{n}_i) = T(\theta_o) S'(\boldsymbol{p}, \boldsymbol{p}_i; \boldsymbol{n}, \boldsymbol{n}_i) T(\theta_i) , \qquad (13)$$

where $T(\theta)$ is the Fresnel transmittance for unpolarized light from the air at incident angle θ, $\theta_i = \cos^{-1}(\boldsymbol{n}_i \cdot \boldsymbol{L})$, $\theta_o = \cos^{-1}(\boldsymbol{n} \cdot \boldsymbol{V})$, and $S'(\boldsymbol{p}, \boldsymbol{p}_i; \boldsymbol{n}, \boldsymbol{n}_i)$ represents scattering and absorption. Note that our model is a BRDF and not a Bidirectional Subsurface Scattering Reflectance Distribution Function (BSSRDF) [20] as $\boldsymbol{p}$ and $\boldsymbol{p}_i$ are on the same surface patch. In contrast to the BRDF approximation of the BSSRDF proposed by Jensen *et al.* [12], in our model, $T(\theta_i)$ and $T(\theta_o)$ depend on the microfacet.

When the light source direction is $\boldsymbol{L}$, we obtain the incident flux $d\Phi_i(\boldsymbol{p}_i; \boldsymbol{n}_i)$ as

$$d\Phi_i(\boldsymbol{p}_i; \boldsymbol{n}_i) = G_s^b(\boldsymbol{p}_i; \boldsymbol{n}_i) \cdot (\boldsymbol{n}_i \cdot \boldsymbol{L}) E_o dA_{\boldsymbol{n}_i} , \qquad (14)$$

where $G_s^b(\boldsymbol{p}_i; \boldsymbol{n}_i)$ is a binary shadowing function at $\boldsymbol{p}_i$. From Eqs. (6) and (8) to (14) the projected radiance $L_{rp}(\boldsymbol{n})$ becomes

$$L_{rp}(\boldsymbol{n}) = \frac{\boldsymbol{n} \cdot \boldsymbol{V}}{(\boldsymbol{n} \cdot \boldsymbol{N})(\boldsymbol{N} \cdot \boldsymbol{V})} T(\theta_o)$$
$$\int_\Omega M(\boldsymbol{n}, \boldsymbol{n}_i) T(\theta_i)(\boldsymbol{L} \cdot \boldsymbol{n}_i) |A_p| D(\theta_{\boldsymbol{n}_i}) d\omega_{\boldsymbol{n}_i} \cdot E_o , \qquad (15)$$

where

$$M(\boldsymbol{n}, \boldsymbol{n}_i) = \frac{1}{|A_{\boldsymbol{n}}||A_{\boldsymbol{n}_i}|} \int_{A_{\boldsymbol{n}}} \int_{A_{\boldsymbol{n}_i}} G_m^b(\boldsymbol{p}) G_s^b(\boldsymbol{p}_i) S'(\boldsymbol{p}, \boldsymbol{p}_i) dA_{\boldsymbol{n}_i} dA_{\boldsymbol{n}} . \qquad (16)$$

For simplicity, we omit $\boldsymbol{n}$ and $\boldsymbol{n}_i$ from the notations for G_m^b, G_s^b, and S'. From Eq. (16), $M(\boldsymbol{n}, \boldsymbol{n}_i)$ denotes the average of the product of $G_m^b(\boldsymbol{p})$, $G_s^b(\boldsymbol{p}_i)$ for all combinations of light transport $S'(\boldsymbol{p}, \boldsymbol{p}_i)$ between surface points $\boldsymbol{p}$ and $\boldsymbol{p}_i$ on microfacets oriented to $\boldsymbol{n}$ and $\boldsymbol{n}_i$ respectively.

We provide a detailed analysis of this novel masking and shadowing term $M(\boldsymbol{n}, \boldsymbol{n}_i)$ that takes into account light transport between microfacets $S'(\boldsymbol{p}, \boldsymbol{p}_i)$ in the supplementary material. Through this analysis, we show that it can be simply computed as

$$M(\boldsymbol{n}, \boldsymbol{n}_i) = G_m(\boldsymbol{n}) G_s(\boldsymbol{n}_i) \overline{S'}(\boldsymbol{n}, \boldsymbol{n}_i) , \qquad (17)$$

where $G_m(\boldsymbol{n})$, $G_s(\boldsymbol{n}_i)$, and $\overline{S'}(\boldsymbol{n}, \boldsymbol{n}_i)$ are the average of $G_m^b(\boldsymbol{p})$, $G_s^b(\boldsymbol{p}_i)$, and $S'(\boldsymbol{p}, \boldsymbol{p}_i)$ for $\boldsymbol{p}$ and $\boldsymbol{p}_i$, respectively. The light transport $\overline{S'}(\boldsymbol{n}, \boldsymbol{n}_i)$ does not depend on $\boldsymbol{L}$ and $\boldsymbol{V}$. For consistency with surface reflection, we use Smith's masking-shadowing function for $G_m(\boldsymbol{n})$ and $G_s(\boldsymbol{n}_i)$ [8, 27].

The light transport $\overline{S'}(\boldsymbol{n}, \boldsymbol{n}_i)$ follows the energy conservation law. Since $\overline{S'}(\boldsymbol{n}, \boldsymbol{n}_i)$ does not depend on $\boldsymbol{L}$ and $\boldsymbol{V}$, energy conservation law becomes

$$\pi \int_\Omega \overline{S'}(\boldsymbol{n}, \boldsymbol{n}_i) \cdot \frac{|A_{\boldsymbol{n}}|}{d\omega_{\boldsymbol{n}}} d\omega_{\boldsymbol{n}} = k_b , \qquad (18)$$

where k_b is the body reflection albedo, π is the sum of energy to all directions, and the integration represents the sum of energy at all points. We assume that k_b is constant for the surface patch. Although k_s does not depend on the color of the surface, k_b depends on it due to absorption in the subsurface (*i.e.*, dichromatic reflectance model [26]).

Let us introduce a microfacet correlation function $f(\boldsymbol{n}, \boldsymbol{n}_i)$ to interpret Eq. (18)

$$\overline{S'}(\boldsymbol{n}, \boldsymbol{n}_i) = \frac{k_b}{|A_p|\pi} f(\boldsymbol{n}, \boldsymbol{n}_i) . \qquad (19)$$

From Eqs. (7), (18) and (19), $f(\boldsymbol{n}, \boldsymbol{n}_i)$ is normalized by

$$\int_\Omega f(\boldsymbol{n}, \boldsymbol{n}_i) D(\theta_{\boldsymbol{n}}) d\omega_{\boldsymbol{n}} = 1 . \qquad (20)$$

The microfacet correlation function $f(\boldsymbol{n}, \boldsymbol{n}_i)$ encodes the spatial bias of the microfacet orientation distribution. For example, if most microfacets oriented near $\boldsymbol{n}_i$ are located near microfacets with $\boldsymbol{n}_i$, $f(\boldsymbol{n}, \boldsymbol{n}_i)$ becomes an angularly narrow distribution function. In the case of randomly distributed microfacets, $f(\boldsymbol{n}, \boldsymbol{n}_i)$ become the uniform distribution function. Since the biased microfacet distributions compose the mesoscopic surface, $f(\boldsymbol{n}, \boldsymbol{n}_i)$ also represents

the mesoscopic surface geometry. When $f(\boldsymbol{n}, \boldsymbol{n}_i)$ is the uniform distribution, the incident light is distributed to microfacets oriented in any direction uniformly and reflected light is hardly directional, *i.e.* the gross body reflection is similar to Lambertian. On the other hand, when $f(\boldsymbol{n}, \boldsymbol{n}_i)$ is an angularly narrow distribution, the incident light is distributed within the same mesogeometry and the reflected light is directional to the incident direction, *i.e.* it behaves similarly to the Oren-Nayar model.

We model the microfacet correlation function with a 3D von Mises–Fisher distribution re-normalized by Eq. (20)

$$f(\boldsymbol{n}, \boldsymbol{n}_i; \kappa) \propto \exp\left[\kappa(\boldsymbol{n}_i \cdot \boldsymbol{n})\right] , \quad (21)$$

where κ is the concentration parameter.

From Eqs. (4), (15), (17) and (19), we obtain the body reflection for the same general microgeometry of surface reflection (Eqs. (1) and (2))

$$L_b(\boldsymbol{N}, \boldsymbol{L}, \boldsymbol{V}) = \frac{1}{\boldsymbol{N} \cdot \boldsymbol{V}} \int_\Omega \int_\Omega G_m(\boldsymbol{n}) D(\theta_{\boldsymbol{n}}) T(\theta_o)(\boldsymbol{V} \cdot \boldsymbol{n}) \cdot$$

$$\frac{k_b}{\pi} f(\boldsymbol{n}, \boldsymbol{n}_i) \cdot G_s(\boldsymbol{n}_i) D(\theta_{\boldsymbol{n}_i}) T(\theta_i)(\boldsymbol{L} \cdot \boldsymbol{n}_i) d\omega_{\boldsymbol{n}} d\omega_{\boldsymbol{n}_i} \cdot E_o . \quad (22)$$

4. Polarimetric Fresnel Microfacet BRDF

Let us now extend the radiometric model to a full polarimetric model. By carefully deriving the Fresnel reflection and transmittance on microgeometry, we show that the polarimetric behavior embodies distinct signatures of the underlying microgeometry in its reflection. For primers on polarization, including Stokes vector and Mueller matrix, please see the supplemental material.

To express the polarization direction, we need to define the coordinate system (CS) of incident light (incident CS) and reflected light (outgoing CS). We define the z-axis of each CS as $\boldsymbol{L}$ and $-\boldsymbol{V}$. The x-axis and y-axis of each CS can be defined arbitrarily for different purposes. We denote them as $\boldsymbol{x}_{\{i,o\}}$ and $\boldsymbol{y}_{\{i,o\}}$, respectively.

4.1. Polarimetric Microfacet Surface Reflection

For surface reflection, we can follow the polarimetric specular BRDF model by Baek *et al.* [2]. To consider polarization, the Fresnel reflectance in Eq. (1) is replaced with the Mueller matrix of surface reflection $\boldsymbol{R}$, which consists of Fresnel coefficients determined by the incident angle θ_d and the index of refraction μ, and a rotation matrix $\boldsymbol{C}$ that represents the polarization direction. Due to limited space, these Mueller matrices are shown in the supplemental material. The Stokes vector of surface reflection $\boldsymbol{s}_s$ becomes

$$\boldsymbol{s}_s = k_s \frac{D(\theta_{\boldsymbol{H}}) G(\boldsymbol{H})}{4(\boldsymbol{N} \cdot \boldsymbol{V})} \boldsymbol{C}(\varphi_{o,s}) \boldsymbol{R}(\theta_d) \boldsymbol{C}(-\varphi_{i,s}) \boldsymbol{s}_i , \quad (23)$$

where $\varphi_{\{i,o\},s}$ is the angle between the $\boldsymbol{y}_{\{i,o\}}$ and the microfacet normal $\boldsymbol{H}$ projected onto $\boldsymbol{x}_{\{i,o\}} \boldsymbol{y}_{\{i,o\}}$-plane, and $\boldsymbol{s}_i$ is the Stokes vector of the incident light.
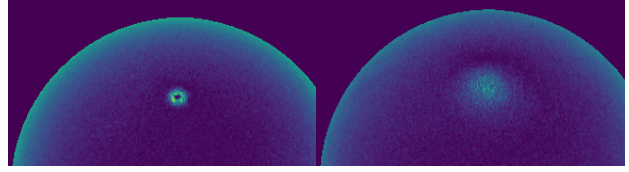

Figure 3. Our FMBRDF provides intuitive interpretations of surface reflection polarization, particularly of its degree of polarization. See text for details.

4.2. Polarimetric Microfacet Body Reflection

We need to express the body reflection Eq. (22) as the aggregated retransmitted light from the oriented mirror microfacets with a Stokes vector and Mueller matrix. The polarization is transformed by the transmission, scattering in the subsurface, and then the retransmission into air. The Mueller matrices of Fresnel transmission $\boldsymbol{T}$, which consists of Fresnel coefficients, and depolarization by subsurface scattering $\boldsymbol{D}_p$ are shown in the supplemental material. Replacing $T(\theta_o)$, $T(\theta_i)$, and $\frac{k_b}{\pi}$ in Eq. (22) with $\boldsymbol{C}(\varphi_{o,b}) \boldsymbol{T}(\theta_o)$, $\boldsymbol{T}(\theta_i) \boldsymbol{C}(\varphi_{i,b})$, and $\boldsymbol{D}_p\left(\frac{k_b}{\pi}\right)$, the Stokes vector of body reflection $\boldsymbol{s}_b$ becomes

$$\boldsymbol{s}_b = \frac{1}{\boldsymbol{N} \cdot \boldsymbol{V}} \int_\Omega \int_\Omega G_m(\boldsymbol{n}) D(\theta_{\boldsymbol{n}})(\boldsymbol{V} \cdot \boldsymbol{n}) \boldsymbol{C}(\varphi_{o,b}) \boldsymbol{T}(\theta_o) \cdot \boldsymbol{D}_p\left(\frac{k_b}{\pi}\right)$$

$$f(\boldsymbol{n}, \boldsymbol{n}_i) \cdot G_s(\boldsymbol{n}_i) D(\theta_{\boldsymbol{n}_i})(\boldsymbol{L} \cdot \boldsymbol{n}_i) \boldsymbol{T}(\theta_i) \boldsymbol{C}(\varphi_{i,b}) d\omega_{\boldsymbol{n}} d\omega_{\boldsymbol{n}_i} \cdot \boldsymbol{s}_i . \quad (24)$$

where $\varphi_{\{i,o\},b}$ is the angle between $\boldsymbol{y}_{\{i,o\}}$ and $\boldsymbol{n}_i$ and $\boldsymbol{n}$ projected onto the $\boldsymbol{x}_{\{i,o\}} \boldsymbol{y}_{\{i,o\}}$-plane.

4.3. Polarimetric Interpretation

As our FMBRDF model is physically-based, it provides an intuitive interpretation of polarization of surface reflection. Polarimetric image interpretation is notoriously difficult but our model lets us map key characteristics to its physically explicable parameters. As shown in Fig. 3, let us consider the degree of linear polarization (DoLP) of a sphere, *i.e.*, an object that has all possible frontal facing surface normals. The roughness and shape of the microfacet orientation distribution function dictate the DoLP distribution on the surface. The further the surface normal is from the half vector, the more the observed surface reflection light attenuates and the smaller the DoLP as body reflection dampens the polarization by surface reflection. This relation of the DoLP and the angle between the half vector and surface normal $\theta_{\boldsymbol{H},\boldsymbol{n}}$ embodies the shape β of the distribution function. The roughness is encoded in the width of this DoLP lobe for $\theta_{\boldsymbol{H},\boldsymbol{n}}$. The index of refraction determines the Fresnel transmittance, which in turn governs the DoLP of the region dominated by body reflection. The albedo ratio $r_k = \frac{k_b}{k_s}$ determines the scale of the DoLP lobe for $\theta_{\boldsymbol{H},\boldsymbol{n}}$. The microfacet correlation parameter κ controls
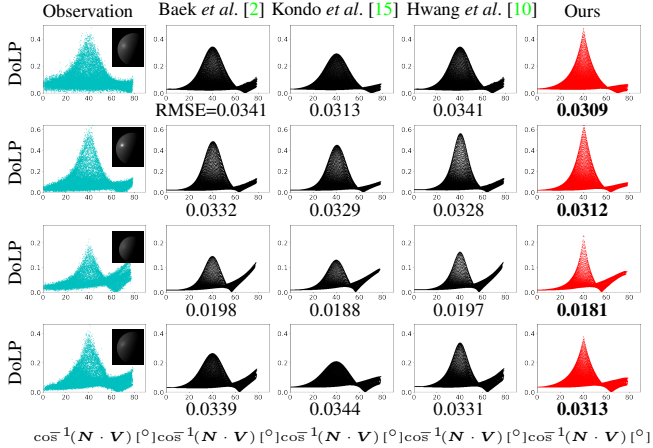
Figure 4. Polarimetric accuracy shown with DoLP values plotted as a function of the angle between the global surface normal and the viewing direction. Each graph shows the fitting results for one of the lighting conditions. The number under the graph is the root mean square error. Our FMBRDF model accurately captures the characteristics of the DoLP distributions both for surface and body reflections regardless of the surface roughness and color.
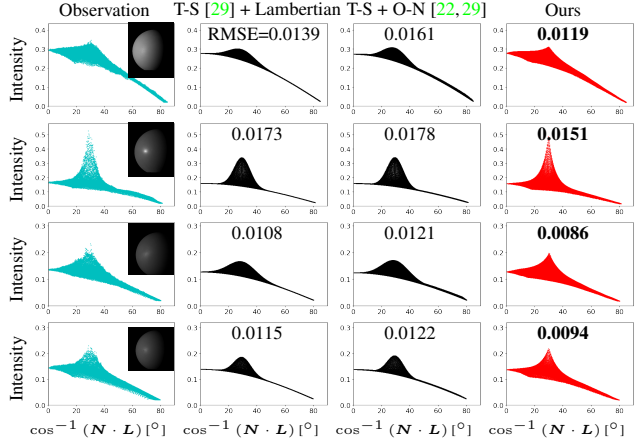

Figure 5. Radiometric accuracy shown with intensity values as a function of the angle between the global surface normal and the light source direction. Each graph shows the fitting results for one of the lighting conditions. The number at the top of the graph is the RMSE. Our FMBRDF model accurately represents both surface and body reflections regardless of the surface roughness and color.

the DoLP of body reflection in surface areas whose global surface normal is aligned with the lighting direction. For instance, when κ is large, the polarization by the microfacets aligned with the global surface normal is dampened less by light from other microfacets.

5. Polari-Radiometric Reflectometry

The newly derived FMBRDF describes both the polarimetric and radiometric behaviors of light reflected by a surface. This allows us to estimate its parameters from a single polarimetric image captured with a known directional light of an object of known geometry and then use those parameters to analyze and synthesize not just polarimetric but also radiometric appearance of that surface.

Given a single polarimetric image, the parameters of FMBRDF, namely the index of refraction μ, albedo ratio $r_k = \frac{k_b}{k_s}$, surface reflection albedo k_s, surface roughness α, and shape of orientation distribution β, can be estimated with least squares optimization

$$\min_{\mu, r_k, k_s, \alpha, \kappa} \frac{1}{M} \sum_i^M (\bar{I}_i - I_i)^2 + \frac{\sum_i^M w_i(\bar{\rho}_i - \rho_i)^2}{\sum_i^M w_i} \,, \quad (25)$$

where $\bar{\rho}_i$ and ρ_i are the observed and rendered (*i.e.*, computed with FMBRDF) DoLPs at pixel i, respectively, $\bar{I}_i$ and I_i are the observed and rendered intensity at pixel i, respectively, and M is the number of pixels. The weight w_i is set to the ratio of the number of inliers and outliers when pixel i is an outlier, and 1 otherwise, to account for the imbalance in the surface areas dominated with surface or body

reflection. We avoid the costly integration of body reflection and Smith's masking function by approximating each with a simple multi-layer perceptron (MLP) and leverage their fast inference and differentiability. We solve the non-linear optimization using Adam [13].

6. Experimental Results

We evaluate the effectiveness of our model by examining its accuracy in expressing real-world surface appearance both in polarimetry and radiometry. We also show that our FMBRDF can be estimated from a single polarimetric image under a known directional light. For all experiments, input images are captured with a commercial monochrome polarization camera (Lucid TRI050S-PC) that uses quad-Bayer polarization filter chips (Sony IMX250MZR). In the supplemental material, we also demonstrate the use of FM-BRDF for joint reflectance and geometry recovery.

6.1. Polarimetric Model Accuracy

We first evaluate the polarimetric accuracy of FMBRDF using polarimetric images of real surfaces with known surface normals. In particular, we use spheres captured under various lighting conditions and evaluate the accuracy of FMBRDF and other existing pBRDF models in fitting the DoLP values. Figure 4 shows the DoLP values on the surface as a function of the angle between the global surface normal and the viewing direction for the input polarization observation, our model, and representative physically-based pBRDF models. It clearly shows that our FMBRDF model accurately explains the DoLP for all surface normals for various materials of different surface roughnesses. Other
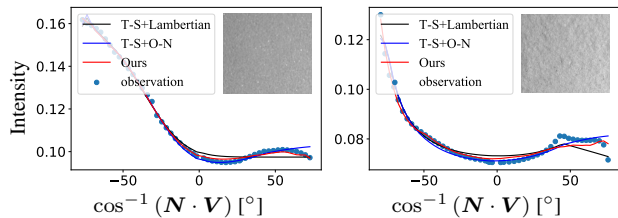
Figure 6. Radiometric fitting results on objects with non-Lambertian diffuse reflectance. The microfacet correlation function enables our model to represent Oren-Nayar diffuse reflection caused by rough mesogeometry.

pBRDF models result in large errors for rougher surfaces as they do not model the microfacet body reflection.

6.2. Radiometric Model Accuracy

We evaluate the radiometric accuracy of our FMBRDF model by fitting our model and others to images of real surfaces. Figure 5 shows the results of our FMBRDF and other radiometric BRDF models on several images taken under different light source directions. These results clearly show that a Gaussian microfacet distribution is hardly appropriate for real-world surfaces. Furthermore, our FMBRDF model can represent observed body reflection more accurately than the Lambertian and Oren-Nayar models.

Our FMBRDF model subsumes the Oren-Nayar diffuse reflection model as a special case when the concentration parameter κ of the microfacet correlation function is large. We capture a planar sample with rough mesogeometry by rotating the camera around it. The global surface normal N, the viewing direction V, and the light source direction L are on the same plane. We compute the average intensity over all pixels within the surface region shared across all images. Figure 6 shows the fitting results of our FM-BRDF and other radiometric BRDFs. The results show that our model can represent non-Lambertian diffuse reflection including Oren-Nayar diffuse reflection, in particular with its microfacet correlation function. Please see the supplemental material for more results.

6.3. Polari-Radiometric Reflectometry Accuracy

Now, we estimate our FMBRDF from a single polarimetric image of an object with known geometry by solving Eq. (25). We quantitatively evaluate the accuracy of the estimated FMBRDF by rendering a radiometric image under a novel lighting condition. Figure 7 shows rendered images under novel lighting conditions and prediction errors of FM-BRDF and other physically-based BRDF models for objects of different color, surface roughness, and shape. The parameters of the other models and ours only radiance are estimated from the observed radiance values. Ours only polarization is estimated from only DoLPs. Radiometric BRDF
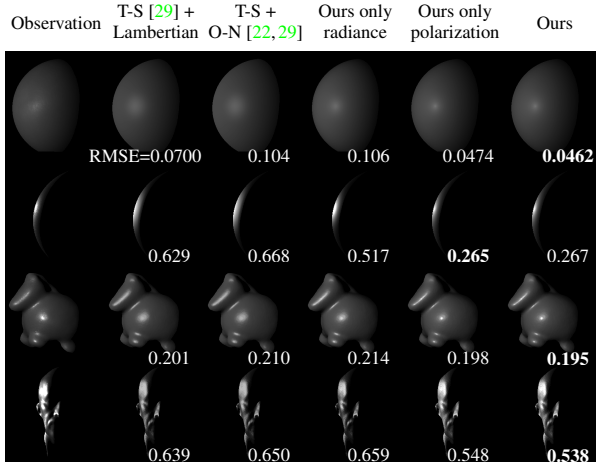

Figure 7. Radiometric renderings using BRDF parameters estimated from single polarimetric images (ours), DoLP images (ours only polarization), and radiometric images (others). The number under the rendered image is the RMSE from the observation divided by the average of observed radiance. In contrast to BRDFs estimated with only radiance, FMBRDF estimated with radiance and polarization results in accurate radiometric appearance both in surface and body reflection for different surfaces.

models, including ours when estimated from observed radiance, fail to accurately predict the surface reflection. In contrast, images rendered with FMBRDF using parameter estimates from polarization are accurate, especially near the highlights regardless of the albedo ratio, roughness, and shape of the object. These results clearly demonstrate the accuracy of polari-radiometric reflectometry and the advantage of FMBRDF which enables it by unifying radiometric and polarimetric reflection.

7. Conclusion

In this paper, we derived Fresnel Microfacet BRDF, a novel analytical reflectance model that is physically accurate and generalizes to various real-world surfaces. FM-BRDF models body and surface reflection with the same microgeometry represented with an oriented distribution of mirror microfacets and also unifies radiometric and polarimetric behaviors of the reflections in a single model. This resolves the physical implausibility of traditional diffuse plus specular reflection models widely adopted in computer vision and enables accurate and robust reflectance estimation for a wide range of real-world surfaces. We believe FMBRDF will serve as a sound, versatile reflectance model for radiometric and polarimetric image understanding.

References

[1] Gary A. Atkinson and Edwin R. Hancock. Shape Estimation Using Polarization and Shading from Two Views. *IEEE TPAMI*, 29, 2007. 3

[2] Seung-Hwan Baek, Daniel S. Jeon, Xin Tong, and Min H. Kim. Simultaneous Acquisition of Polarimetric SVBRDF and Normals. *ACM TOG*, 37:1 – 15, 2018. 1, 2, 3, 6, 7

[3] Seung-Hwan Baek, Tizian Zeltner, Hyunjin Ku, Inseung Hwang, Xin Tong, Wenzel Jakob, and Min H Kim. Image-Based Acquisition and Modeling of Polarimetric Reflectance. *ACM TOG*, 39(4):139, 2020. 3

[4] Zhe Chen, Shohei Nobuhara, and Ko Nishino. Invertible Neural BRDF for Object Inverse Rendering. In *ECCV*, 2020. 3

[5] Robert L Cook and Kenneth E. Torrance. A Reflectance Model for Computer Graphics. *ACM TOG*, 1(1):7–24, 1982. 2, 3

[6] Kristin Dana, Bram van Ginneken, Shree K. Nayar, and Jan J. Koenderink. Reflectance and Texture of Real-World Surfaces. *ACM TOG*, 18(1):1–34, Jan. 1999. 4

[7] Dave Edwards, Solomon Boulos, Jared Johnson, Peter Shirley, Michael Ashikhmin, Michael Stark, and Chris Wyman. The Halfway Vector Disk for BRDF Modeling. *ACM TOG*, 25(1):1–18, 2006. 2

[8] Eric Heitz. Understanding the Masking-Shadowing Function in Microfacet-Based BRDFs. *Journal of Computer Graphics Techniques (JCGT)*, 3(2):48–107, June 2014. 4, 5

[9] Nicolas Holzschuch and Romain Pacanowski. A Two-Scale Microfacet Reflectance Model Combining Reflection and Diffraction. *ACM TOG*, 36(4), jul 2017. 3, 4

[10] Inseung Hwang, Daniel S Jeon, Adolfo Muñoz, Diego Gutierrez, Xin Tong, and Min H Kim. Sparse Ellipsometry: Portable Acquisition of Polarimetric SVBRDF and Shape with Unstructured Flash Photography. *ACM TOG*, 41(4):1–14, 2022. 3, 7

[11] Milo W Hyde IV, Jason D Schmidt, and Michael J Havrilla. A geometrical optics polarimetric bidirectional reflectance distribution function for dielectric and metallic surfaces. *Optics express*, 17(24):22138–22153, 2009. 3

[12] Henrik Wann Jensen, Stephen R. Marschner, Marc Levoy, and Pat Hanrahan. A Practical Model for Subsurface Light Transport. In *Proceedings of the 28th Annual Conference on Computer Graphics and Interactive Techniques*, SIGGRAPH '01, page 511–518, New York, NY, USA, 2001. Association for Computing Machinery. 5

[13] Diederik P. Kingma and Jimmy Ba. Adam: A Method for Stochastic Optimization. In Yoshua Bengio and Yann LeCun, editors, *3rd International Conference on Learning Representations, ICLR 2015, San Diego, CA, USA, May 7-9, 2015, Conference Track Proceedings*, 2015. 7

[14] Jan J. Koenderink and Andrea J. Van Doorn. Phenomenological description of bidirectional surface reflection. *JOSA A*, 15:2903–2912, 1998. 2

[15] Yuhi Kondo, Taishi Ono, Legong Sun, Yasutaka Hirasawa, and Jun Murayama. Accurate Polarimetric BRDF for Real Polarization Scene Rendering. In *ECCV*, pages 220–236. Springer, 2020. 3, 7

[16] Eric PF Lafortune, Sing-Choong Foo, Kenneth E Torrance, and Donald P Greenberg. Non-Linear Approximation of Reflectance Functions. In *Proceedings of the 24th annual conference on Computer graphics and interactive techniques*, pages 117–126, 1997. 2

[17] J.H. Lambert. *Photometria sive de mensura de gratibus luminis colorum et umbrae*. Augsburg, 1760. 1

[18] Wan-Chun Ma, Tim Hawkins, Pieter Peers, Charles-Felix Chabert, Malte Weiss, and Paul E Debevec. Rapid Acquisition of Specular and Diffuse Normal Maps from Polarized Spherical Gradient Illumination. *Rendering Techniques*, 2007(9):10, 2007. 3

[19] Wojciech Matusik. *A Data-Driven Reflectance Model*. PhD thesis, Massachusetts Institute of Technology, 2003. 3

[20] F.E. Nicodemus, J.C. Richmond, J.J. Hsia, W.I. Ginsberg, and T. Limperis. Geometrical Considerations and Nomenclature for Reflectance. *Applied Optics*, 9:1474–1475, 1977. 2, 5

[21] Ko Nishino. Directional Statistics BRDF Model. In *ICCV*, pages 476–483. IEEE, 2009. 3, 4

[22] Michael Oren and Shree K. Nayar. Generalization of the Lambertian Model and Implications for Machine Vision. *International Journal of Computer Vision*, 14:227–251, 1995. 2, 3, 4, 7, 8

[23] Bui Tuong Phong. Illumination for Computer Generated Pictures. *Communications of the ACM*, 18:311 – 317, 1975. 2

[24] Ravi Ramamoorthi and Pat Hanrahan. A Signal-Processing Framework for Inverse Rendering. In *Proceedings of the 28th annual conference on Computer graphics and interactive techniques*, pages 117–128, 2001. 2

[25] Fabiano Romeiro, Yuriy Vasilyev, and Todd Zickler. Passive Reflectometry. In *ECCV*, pages 859–872. Springer, 2008. 3

[26] Steven A Shafer. Using Color to Separate Reflection Components. *Color Research & Application*, 10(4):210–218, 1985. 5

[27] Bruce Smith. Geometrical Shadowing of a Random Rough Surface. *IEEE transactions on antennas and propagation*, 15(5):668–671, 1967. 4, 5

[28] William A. P. Smith, Ravi Ramamoorthi, and Silvia Tozza. Height-from-Polarisation with Unknown Lighting or Albedo. *IEEE TPAMI*, 41(12):2875–2888, 2019. 3

[29] Kenneth E Torrance and Ephraim M Sparrow. Theory for Off-Specular Reflection From Roughened Surfaces. *Josa*, 57(9):1105–1114, 1967. 1, 2, 3, 4, 7, 8

[30] Bruce Walter, Stephen R. Marschner, Hongsong Li, and Kenneth E. Torrance. Microfacet Models for Refraction through Rough Surfaces. In *Proceedings of the 18th Eurographics Conference on Rendering Techniques*, EGSR'07, pages 195–206. Eurographics Association, 2007. 2, 3

[31] Dizhong Zhu and William A. P. Smith. Depth from a polarisation + RGB stereo pair. In *CVPR*, 2019. 3